Zoosymposia 7: 53–70 (2012)
www.mapress.com/zoosymposia/

ISSN 1178-9905 (print edition)
ZOOSYMPOSIA
ISSN 1178-9913 (online edition)

Broad application of non-invasive imaging techniques to echinoids and other echinoderm taxa*

ALEXANDER ZIEGLER

Museum of Comparative Zoology, Department of Organismic and Evolutionary Biology, Harvard University, Cambridge, MA, USA; E-mail: aziegler@fas.harvard.edu

**In*: Kroh, A. & Reich, M. (Eds.) Echinoderm Research 2010: Proceedings of the Seventh European Conference on Echinoderms, Göttingen, Germany, 2–9 October 2010. *Zoosymposia*, 7, xii+316 pp.

Abstract

Tomographic imaging techniques such as micro-computed tomography (µCT) and magnetic resonance imaging (MRI) permit the gathering of digital anatomical data from whole animal specimens non-invasively. The resulting datasets can be used for direct observation of the two-dimensional tomographic image data as well as for manual and semi-automated three-dimensional modelling. Freshly fixed specimens as well as preserved museum material can be successfully analyzed using this approach, giving the zoomorphologist a powerful tool for large-scale comparative studies. In order to demonstrate the principle suitability of non-invasive imaging in echinoderm research, µCT scans of 199 and MRI scans of 92 sea urchin (Echinodermata: Echinoidea) species were acquired, resulting in a total of 203 analyzed echinoid species. The taxa selected represent 50 of the currently recognized 60 extant sea urchin families. The present article lists all species that have been analyzed so far and provides information about the scanning parameters employed for each dataset. Furthermore, the workflow established to generate three-dimensional models of sea urchins is outlined. Using a number of examples from µCT as well as MRI scans performed on echinoids, the potential of the systematic approach described here is highlighted. Finally, the suitability of non-invasive imaging techniques for the study of other echinoderm taxa is assessed based on multimodal datasets of representative species.

Key words: Micro-CT, µCT, MRI, Echinodermata, Echinoidea, imaging, 3D visualization

Introduction

Micro-computed tomography (µCT) and magnetic resonance imaging (MRI) can currently be considered the most promising non-invasive techniques for imaging of whole specimens at the centimeter scale (Walter *et al.* 2010). While MRI provides excellent soft tissue contrast (Jakob 2011), µCT can be used to gather information primarily on hard tissues (Stauber & Müller 2008). Over the course of the last five years, I have employed both methods to visualize soft and hard parts in sea urchins (Echinodermata: Echinoidea). Because µCT and MRI are in principle entirely non-invasive imaging techniques, museum material (including type specimens) was successfully integrated into this study, resulting in an unprecedented taxon sampling for comparative morphological purposes. The acquired datasets can be used for computer-based two-dimensional (2D) as well as three-dimensional (3D) visualization and interaction in real-time. In fact, sea urchins constitute the first metazoan taxon to have been systematically documented on such a broad scale using the two complementary imaging

Accepted by A. Kroh & M. Reich: 6 Oct. 2012; published 12 Dec. 2012

modalities µCT and MRI.

The present article provides an overview of the species that have been scanned so far, and presents visual examples for the properties as well as the quality of the datasets obtained. Furthermore, the approach described here is assessed for its principle suitability for large-scale analyses of the other echinoderm groups, that is, feather stars (Crinoidea), brittle stars (Ophiuroidea), sea stars (Asteroidea), and sea cucumbers (Holothuroidea).

Materials and Methods

Specimens were obtained from various sources, including natural history museums and private collections. Almost all specimens scanned during this study have been (re-)deposited in museum collections after scanning and most of these samples are kept in specially marked containers to facilitate potential future re-scanning. The table in the appendix lists the source for each sample together with the respective catalogue number.

Micro-computed tomography (µCT) scanning was performed at the outstation of the Helmholtz-Zentrum Geesthacht at the Deutsches Elektronen-Synchrotron in Hamburg, Germany and at the Center for Nanoscale Systems in Cambridge, MA, USA. The two scanners used were X-ray tube tomography systems equipped with a tungsten X-ray source (Phoenix Nanotom, GE Sensing & Inspection Technologies, Wunstorf, Germany and X-TEK HMX-ST 225, Nikon Metrology, Leuven, Belgium). The parameters of the scanning protocols were: 90–120 kV source voltage, 80–160 µA source current, 0.1–0.2 mm copper filter, 750–2,000 ms exposure time, 1–3 frames averaged, 1–2 frames skipped, 1,200–3,200 frames acquired over 360°, 2,304 x 2,304 and 2,000 x 2,000 pixel detector size, and about 50 min to 2 h 10 min scan time. Reconstruction was performed with and without compression (2x binning) using the software provided with the scanner (*i.e.*, DatosX Reconstruction 1.5 in case of the Phoenix system and Metris XT 2.2 in case of the X-TEK system). Compressed datasets with doubled voxel resolution were created to facilitate rapid access to the raw data (Ziegler & Menze in press). These compressed datasets were about 0.5 to 4 GB large, whereas the uncompressed datasets had individual sizes of about 6 to 30 GB. The table in the appendix lists the voxel resolution of the uncompressed dataset for each specimen.

Magnetic resonance imaging (MRI) using 3D scanning protocols was performed at the Charité-Universitätsmedizin Berlin, Germany, the Institut für Klinische Radiologie in Münster, Germany, and at the Physikalisches Institut in Würzburg, Germany using horizontal-bore small animal scanners with 7 T, 9.4 T, and 17.6 T magnet strength, respectively (Bruker BioSpin GmbH, Ettlingen, Germany). 2D MRI scanning protocols were implemented at the Leibniz-Institut für Molekulare Pharmakologie in Berlin, Germany using a 9.4 T vertical-bore nuclear magnetic resonance scanner equipped for imaging (Bruker BioSpin GmbH, Ettlingen, Germany). Detailed information on sea urchin MRI scanning parameters has been published elsewhere (Ziegler & Mueller 2011; Ziegler *et al.* 2008a). The table in the appendix lists the voxel resolution achieved for each specimen.

The computer equipment used for image reconstruction after µCT and MRI scanning depended on the hardware components provided with the respective scanner. However, all subsequent image analysis and processing was performed using conventional desktop computers. Common specifications for these systems were a 64-bit Windows 7 operating system, a multi-core processor with a minimum

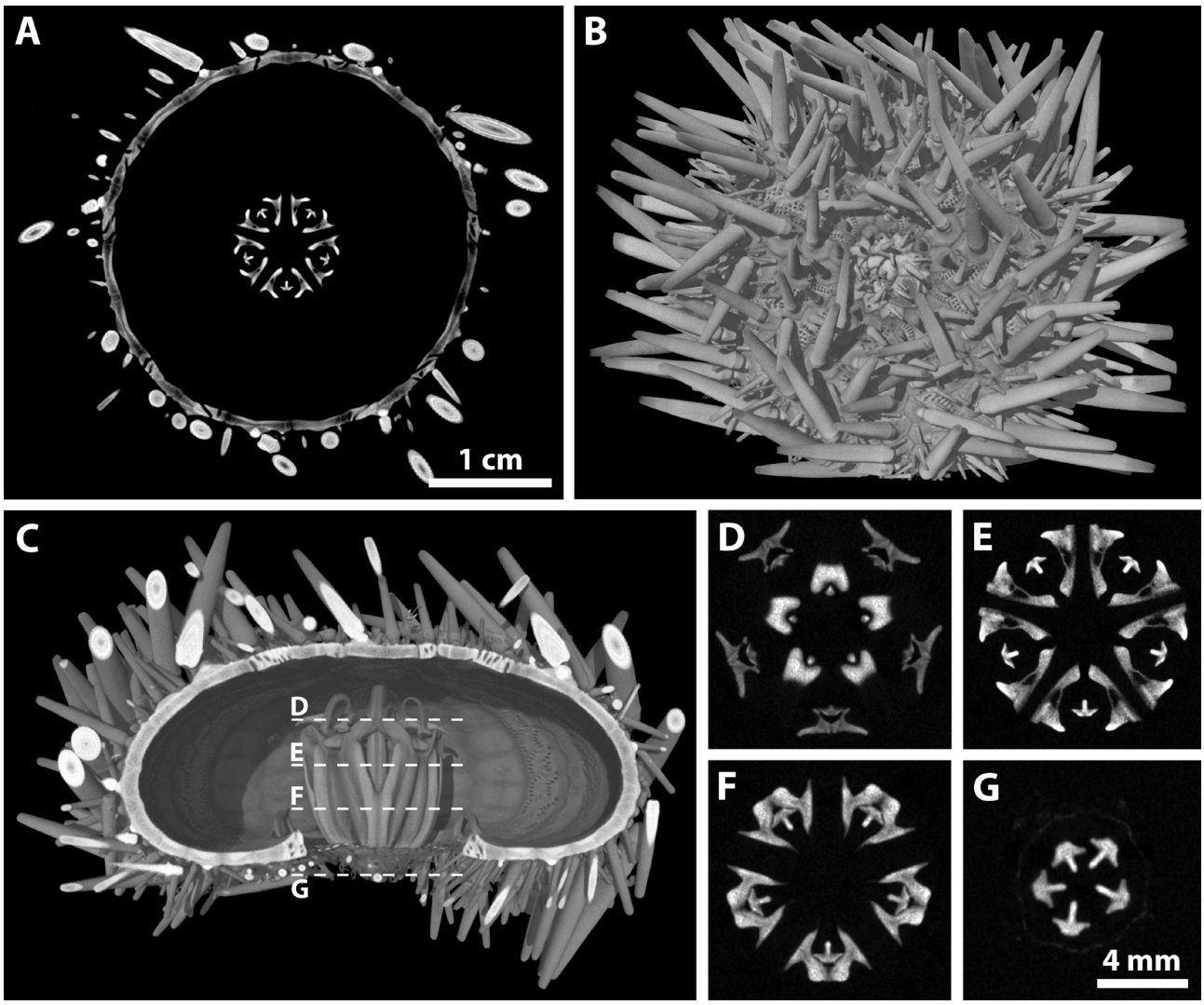

FIGURE 1. Visualization of a micro-computed tomography (µCT) scan of a sea urchin (*Strongylocentrotus purpuratus*). This museum wet specimen, with soft tissues preserved, was scanned directly in ethanol. The voxel resolution of the original dataset is 13.91 µm isotropic, but for reasons of hardware limitations the images shown here are based on the compressed (2x binned) dataset with an isotropic voxel resolution of 27.82 µm. (A) Virtual transverse section at the mid-level of Aristotle's lantern. (B) Aboral view of a volume rendering of the sea urchin's test and spines. Ambulacrum III is facing to the right. (C) Lateral view of a volume rendering of a virtually dissected specimen showing Aristotle's lantern *in situ*. The four virtual transverse sections (D–G) reveal the cross-sectional morphology of the masticatory apparatus of this species. Isotropic tomographic datasets can be virtually sectioned at any given angle and can also be interactively rotated in real-time using the appropriate soft- and hardware.

of 6 GB RAM, and a graphics card with a minimum of 1 GB RAM. Interactive dataset inspection and slicing was accomplished using myVGL 2.1 (Volume Graphics GmbH, Heidelberg, Germany) for µCT datasets and the ImageJ (National Institutes of Health, Bethesda, MD, USA) Volume Viewer plug-in for MRI datasets. Image post-processing was accomplished using Adobe Photoshop and Illustrator CS3 (Adobe Systems, San Jose, CA, USA). 3D volume rendering was performed for all µCT datasets using myVGL 2.1, while MRI datasets were manually segmented and 3D surface rendered using Amira 3, 4, and 5 (Visage Imaging GmbH, Berlin, Germany). Interactive 3D PDF models were created using Adobe 3D Toolkit and Adobe 3D Reviewer (Adobe Systems, San Jose, CA, USA). See Ziegler *et al.* (2011a) for more information on the integration of multimedia files into PDF documents.

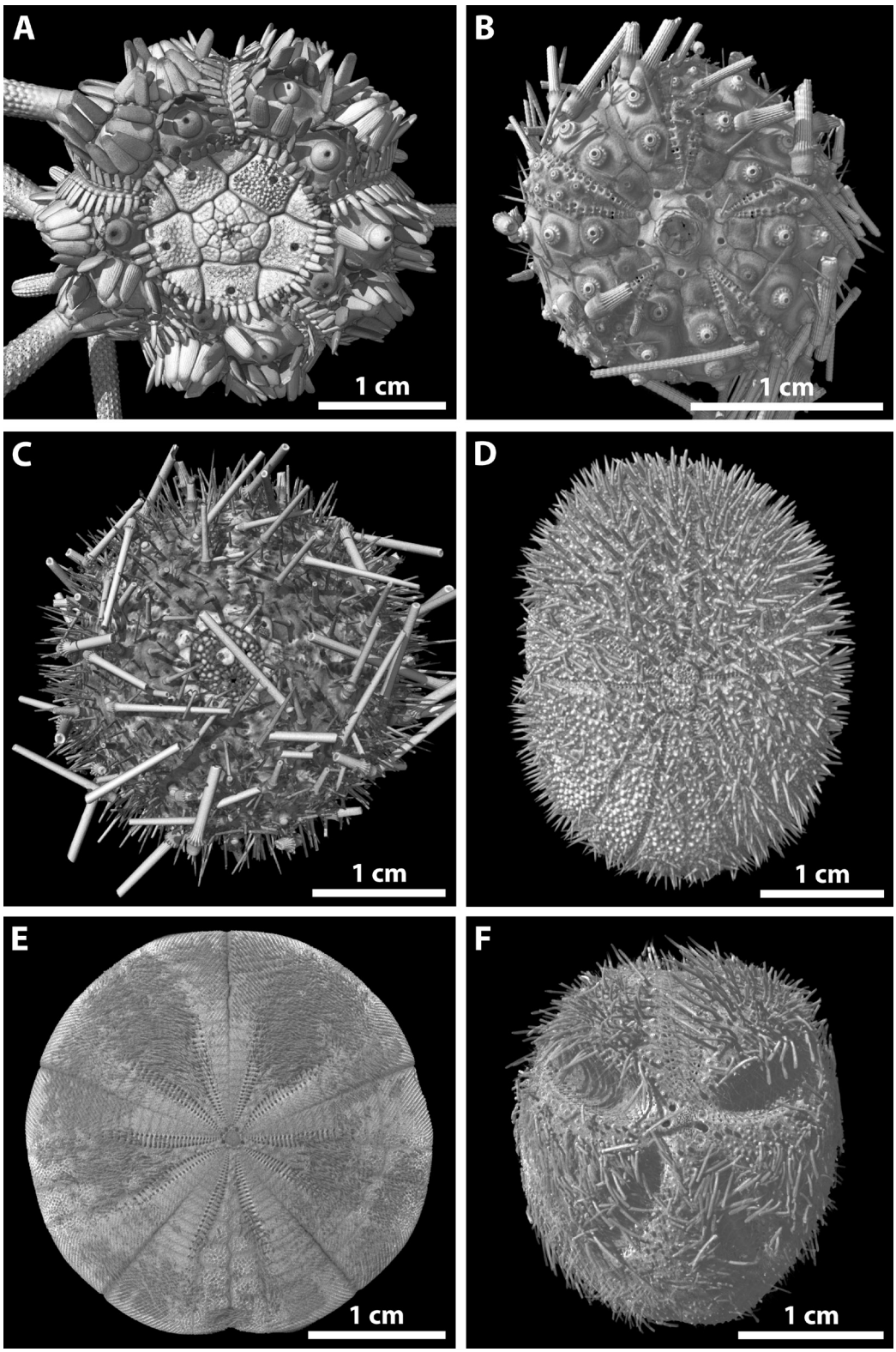

FIGURE 2. Systematic scanning of sea urchins using µCT. This selection of six of the 199 sea urchin species for which µCT scans were gathered shows volume-rendered aboral views of the test with spines. For reasons of hardware limitations, the images depicted here are based on compressed (2x binned) datasets. Ambulacrum III is facing upwards in all images. (A) *Eucidaris metularia* (Cidaridae), a derived cidaroid. (B) *Diadema savignyi* (Diadematidae), a basal 'regular' euechinoid. (C) *Sterechinus agassizii* (Echinidae), a derived echinacean. (D) *Echinoneus cyclostomus* (Echinoneidae), a basal irregular. (E) *Arachnoides placenta* (Clypeasteridae), a clypeasteroid. (F) *Abatus cordatus* (Schizasteridae), a spatangoid. Plate patterns, lantern morphology, and spine architecture are made visible non-invasively using µCT, which opens up the possibility to partly base echinoid taxonomy on this technology in the future. Using µCT, the hard parts of presumably every sea urchin species can be successfully analyzed. Fig. 4 shows complementary, MRI-based models of selected soft tissue structures in combination with virtual transverse sections.

Results

As the aim of this project was to gather tomographic data for comparative morphological purposes, care was taken to cover the full breadth of gross morphological diversity that sea urchins display on the whole. To this end, representative members of as many families as possible were initially selected, while the scanning of one representative member per genus was a later objective. Digital tomographic datasets were finally obtained for 203 sea urchin species (Appendix), with 199 species being scanned using µCT (Figs. 1–2 provide examples) and 92 species being scanned using MRI (see Figs. 3–4 for examples). The specimens selected represent 50 of the currently recognized 60 families of extant sea urchins (Kroh & Mooi 2011).

The workflow established for this study consisted of six consecutive steps. 1) Specimen acquisition: material was either collected in the wild or was loaned from museum collections. Since the objective was to image hard as well as soft structures, primarily wet material with preserved soft tissues was selected. However, dry material was additionally used to increase taxon coverage in cases where no wet specimens were available. In order for the specimens to fit into the scanning chamber, the diameter of each specimen was usually not larger than three cm, although specimens with diameters of up to 20 cm were scanned as well using special scanner setups. In some cases spines had to be removed for tight fit. 2) Specimen preparation: for MRI scanning, specimens were rehydrated and then placed inside containers filled with distilled water, while for µCT scanning specimens were kept in ethanol-filled containers in case of wet material or in air-filled containers in case of dry material. In most cases, the animals were mechanically fixed using plastic or glass rods to prevent movement artifacts during scanning (Ziegler & Mueller 2011). 3) Specimen imaging: once suitable protocols had been established in cooperation with the personnel responsible for the scanner equipment, high-throughput scanning was initiated either in the form of overnight scans (MRI) or during extended scanning sessions (µCT). 4) Dataset processing: in case of MRI, the generated volumetric datasets were transformed to 8-bit TIFF format as well as cropped in their pixel dimensions in order to reduce the final file size, and were then rotated to a standardized orientation using the ImageJ TransformJ plug-in. µCT datasets were reconstructed and then additionally compressed (2x binning) to produce datasets with an individual file size that would be possible to manage interactively on conventional desktop computers, instead of having to rely on high-end visualization clusters (Ziegler *et al.* 2010a). 5) Image analysis: all datasets were repeatedly screened slice by slice for characteristic morphological features. This exploratory approach has so far resulted in MRI-based comparative morphological studies on three internal soft tissue structures: the axial organ (Ziegler *et al.* 2009), the gastric caecum (Rolet *et al.* 2012; Ziegler *et al.* 2010b), and the lantern protractor muscle (Ziegler *et al.* 2012a). In addition, an extended study of sea urchin tooth macro- and microstructure using µCT datasets was initiated (Ziegler *et al.* 2012b). 6) 3D rendering: apart from analyzing the 2D tomographic slices, surface and volume rendered models were produced to study soft and hard parts in 3D. These renderings were threshold-based (*i.e.*, grayscale-dependent) in case of µCT data and segmentation-based (*i.e.*, performed manually) in case of MRI data. To facilitate the communication of complex morphological structures, interactive 3D PDF models were created, some of which are available for download on the Echinoid Directory website (Ziegler *et al.* 2008b) or have been embedded directly into publications (Ziegler *et al.* 2010a, 2010b).

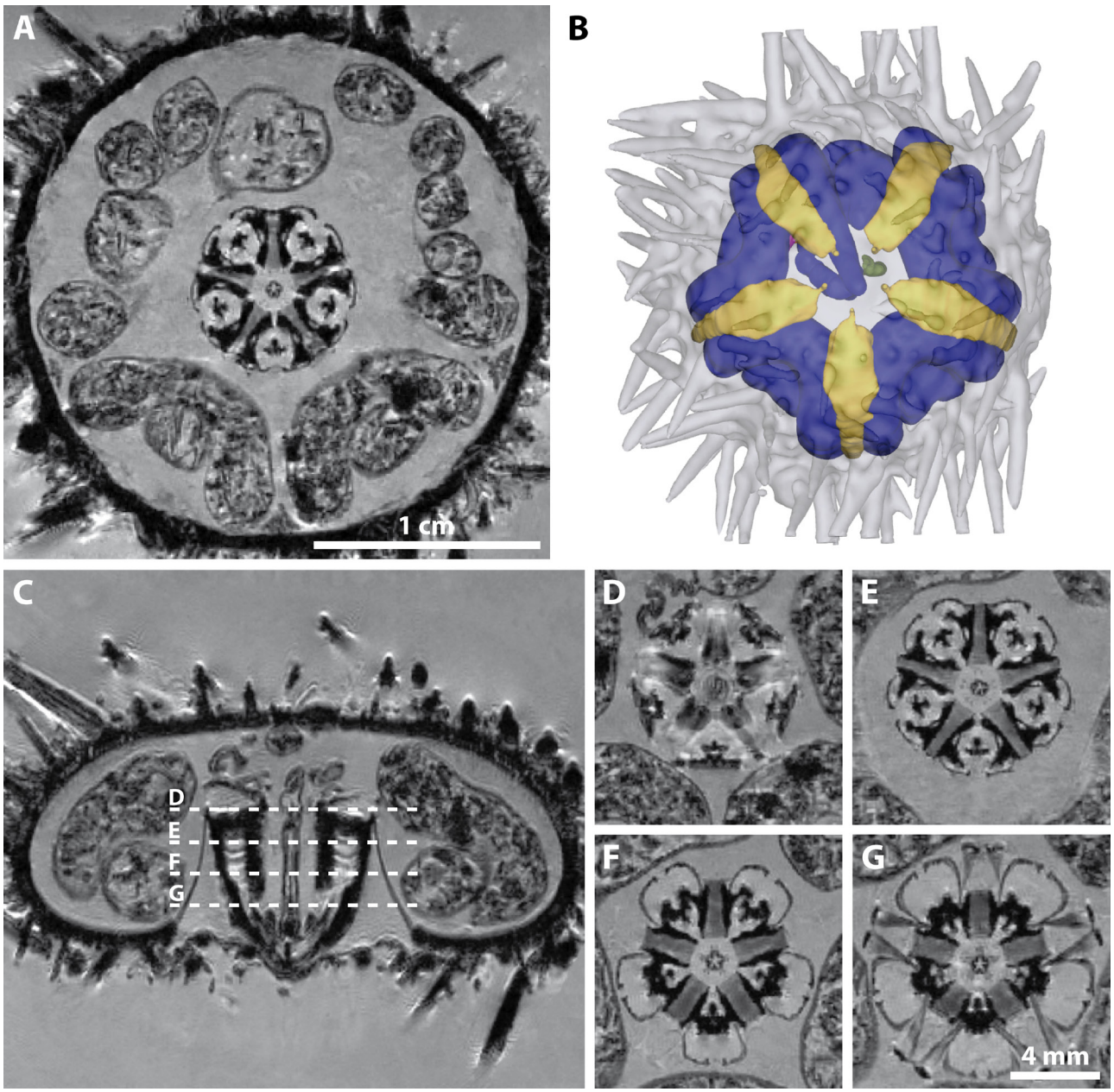

FIGURE 3. Visualization of a magnetic resonance imaging (MRI) scan of a sea urchin (*Strongylocentrotus purpuratus*). This museum wet specimen was scanned in distilled water with a contrast agent added to increase signal strength. The voxel resolution of the dataset is 81 µm isotropic. (A) Virtual transverse section at the mid-level of Aristotle's lantern showing internal organs such as the festooned digestive tract, ampullae, gonads, and lantern muscles. Hard tissue contrast is achieved because of the negative delineation caused by the strong signal from water molecules surrounding calcified elements, which themselves do not generate any signal. (B) Aboral view of a semi-transparent 3D surface rendering of the sea urchin's test showing selected internal organs *in situ*. (C) Longitudinal virtual section through the sample at the level of the pharynx. The four virtual transverse sections (D–G) illustrate the cross-sectional morphology of the masticatory apparatus of this species. Ambulacrum III is facing upwards in all images except in (C). Blue = digestive tract, green = axial complex, grey = endoskeleton, violet = siphon, yellow = gonad.

Discussion

The power of the approach established during this study must be seen in the possibility to conduct large-scale, high-throughput morphological analyses non-invasively. By including museum specimens from collections worldwide, µCT and MRI have enabled the semi-automated, almost industrialized gathering of morphological data from representative members of an entire invertebrate

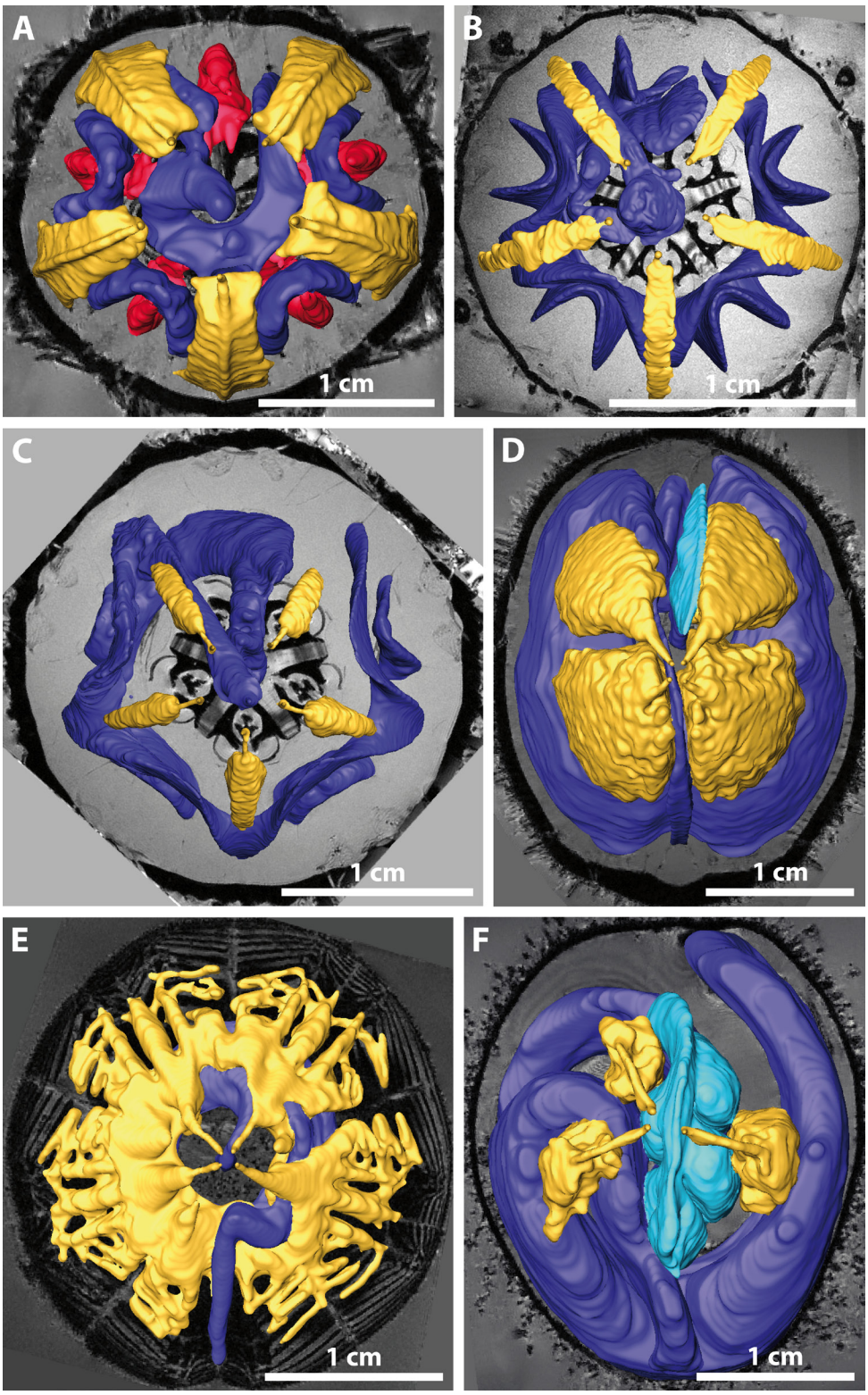

FIGURE 4. Systematic scanning of sea urchins using MRI. This selection of six of the 92 sea urchin species scanned using MRI shows aboral views of 3D surface renderings of selected internal organs in combination with virtual transverse sections through the respective MRI dataset. Ambulacrum III is facing upwards in all images. (A) *Eucidaris metularia* (Cidaridae), a derived cidaroid. (B) *Diadema savignyi* (Diadematidae), a basal 'regular' euechinoid. (C) *Psammechinus miliaris* (Parechinidae), a derived echinacean. (D) *Echinoneus cyclostomus* (Echinoneidae), a basal irregular. (E) *Arachnoides placenta* (Clypeasteridae), a clypeasteroid. (F) *Abatus cavernosus* (Schizasteridae), a spatangoid and congener of *Abatus cordatus* shown in Fig. 2F. Using MRI, most sea urchin species can be successfully analyzed, although some species may ingest large amounts of para- or ferromagnetic sediment that will cause pronounced MRI artifacts. Fig. 2 shows complementary, µCT-based aboral views of test and spines. Blue = digestive tract, cyan = gastric caecum, red = Stewart's organs, yellow = gonad.

taxon. Given the limited funding in taxonomy and systematics, it does not appear unreasonable to predict that the study of many metazoan taxa will be carried out in this way already within the near future (MacLeod *et al.* 2010). Although this study focused on the analysis of extant echinoid taxa, non-invasive imaging techniques, in particular µCT, can be applied to the study of fossil echinoderms as well (Dominguez *et al.* 2002; Rahman & Clausen 2009; Rahman & Zamora 2009; Zamora *et al.* 2012). Despite tremendous technological advances in non-invasive imaging techniques, which are primarily fueled by the application of these techniques in human diagnostics and industrial quality control, a number of aspects remain to be discussed that are of importance for studies of echinoids and other echinoderm taxa.

Although desirable, presumably not all described sea urchin species can be analyzed using the two complementary imaging modalities employed here. This might be due to limitations in specimen availability (some samples may have been lost), specimen size (some samples may be too small or too large for the scanner), specimen properties (some samples may be too fragile to handle), and the occurrence of pronounced artifacts in particular when using MRI (Ziegler & Mueller 2011; Ziegler *et al.* 2011b). In fact, 10 of the currently recognized 60 sea urchin families are not represented in this study for some of the above-mentioned reasons (Appendix). Furthermore, it may become necessary to scan numerous individuals or several ontogenetic stages of a given species in order to fully understand an initial morphological observation, but the required scanning time may not be available or affordable for such projects.

Although MRI and µCT can in principle be considered non-invasive imaging techniques, contrast agents may have to be applied in order to increase signal intensity or to stain soft tissues. For example, in this study Magnevist (BayerSchering, Berlin, Germany) was continuously used during MRI scanning as it improves the signal-to-noise ratio significantly, in turn permitting to achieve higher voxel resolutions (Ziegler *et al.* 2008a; Ziegler *et al.* 2011b). This circumstance, and the fact that about 10 % of the specimens on loan suffered mechanical damage during transport and specimen handling, somewhat qualifies the applicability of the term 'non-invasive'. In addition, the approach advocated here necessitates the comprehensive management of large amounts of digital data (tera- or even petabytes) as well as the availability of sophisticated computer infrastructure.

Nonetheless, MRI and µCT have shown to be valuable tools for studies on sea urchin morphology and the first scans of selected species belonging to the other echinoderm groups reveal that both techniques can be successfully applied to these organisms as well (Figs. 5–6). µCT is particularly well suited for studies on crinoids (Fig. 5A–B, see also Aschauer *et al.* 2010), asteroids (Fig. 5C–D, see also Laforsch *et al.* 2012), and ophiuroids (Fig. 5E–F). In contrast, most holothuroids (Fig. 5G) lack the dense, X-ray-absorbing endoskeleton present in most other echinoderm taxa, making whole specimen scanning using µCT in this group particularly difficult. However, the calcareous ring, for example, constitutes a calcified structure in sea cucumbers that is likely to absorb sufficient X-rays for visualization, while some sea cucumbers (*e.g.*, Psolidae) possess calcareous plates that cover the trunk and that should be well visible in µCT scans. In addition, the application of soft tissue staining techniques (Degenhardt *et al.* 2010; Faraj *et al.* 2009; Jeffery *et al.* 2011; Metscher 2009a, 2009b) could be successfully applied to visualize sea cucumber anatomy, although at current there is no data available regarding potentially detrimental long-term effects of these staining agents on museum material. However, because alpha taxonomy and systematics for most echinoderms are primarily based on hard part morphology, in particular µCT has the potential to become a standard diagnostic tool in echinoderm research. This is especially so in cases where diagnostic characters are accessible

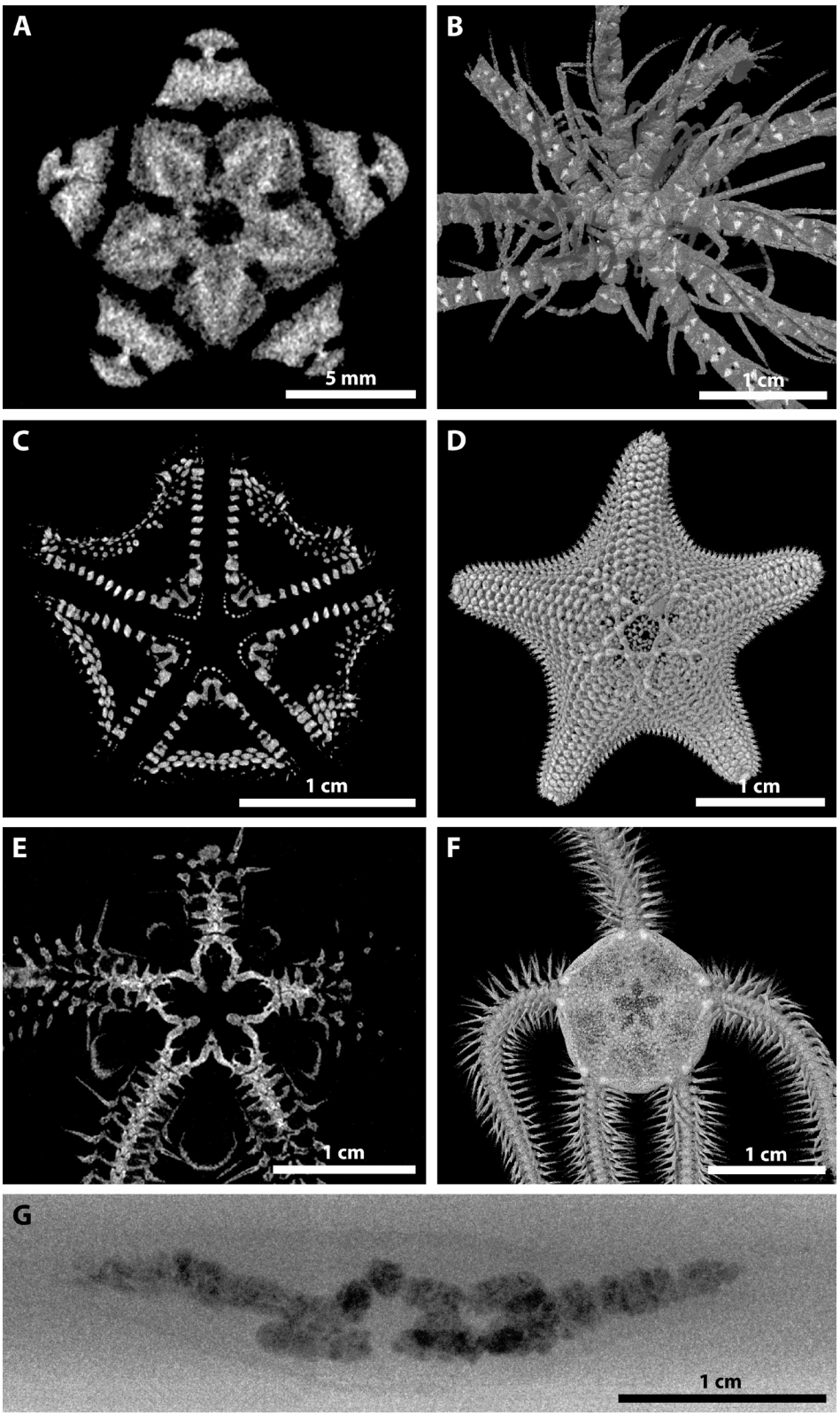

FIGURE 5. Suitability of µCT for its application to further echinoderm taxa. All specimens were scanned in ethanol. (A–B) *Antedon mediterranea* (Antedonidae, ZMH E6859), a feather star (Crinoidea). (C–D) *Asterina gibbosa* (Asterinidae, ZMH E1195), a sea star (Asteroidea). (E–F) *Ophiocoma nigra* (Ophiocomidae, ZMH E2025), a brittle star (Ophiuroidea). (G) *Holothuria pardalis* (Holothuriidae, ZMH E5131), a sea cucumber (Holothuroidea). Location of virtual transverse sections: upper body (A), near mouth (C), at level of bursae (E). In contrast to feather stars, sea stars, and brittle stars, sea cucumbers are only partly suitable for whole specimen scanning using µCT, because of the absence of large amounts of calcified structures. The long dark structure at the center of the 2D X-ray projection shown here (G) is sediment incorporated within the digestive tract. The only slightly X-ray-absorbing integument of this holothuroid species can be seen as a faint outline.

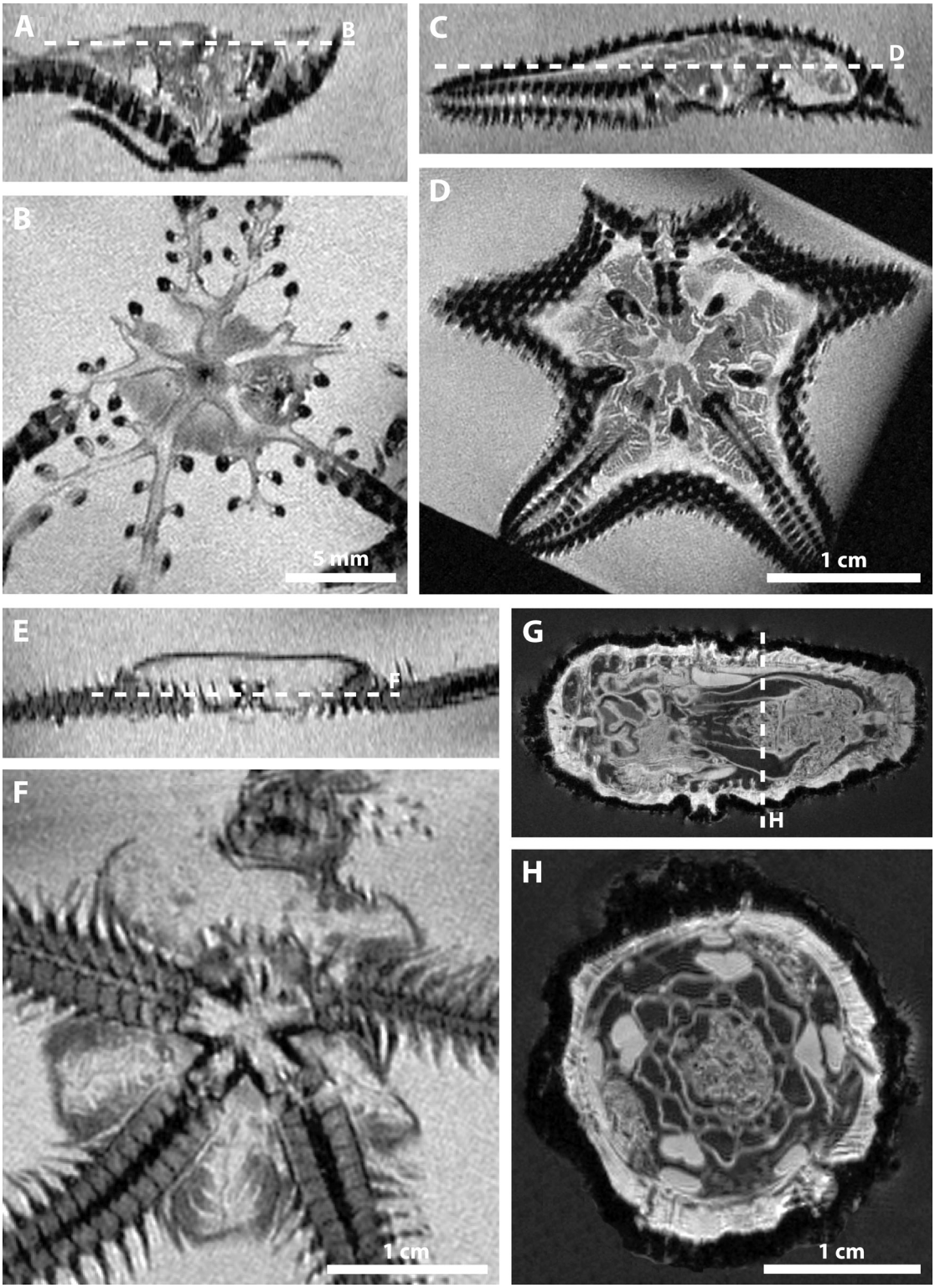

FIGURE 6. Suitability of MRI for its application to further echinoderm taxa. All specimens were scanned in distilled water. The first three specimens (A–F) were scanned with a contrast agent added and using a 2D protocol with 50 x 50 x 200 µm voxel resolution. The fourth specimen (G–H) was scanned without a contrast agent using a 3D protocol with an isotropic voxel resolution of 81 µm. (A–B) *Antedon mediterranea*, a feather star (Crinoidea). (C–D) *Asterina gibbosa*, a sea star (Asteroidea). (E–F) *Ophiocoma nigra*, a brittle star (Ophiuroidea). This specimen had suffered mechanical damage to one of its bursae. (G–H) *Aslia lefevrei* (Cucumariidae), a sea cucumber (Holothuroidea). In principle, all echinoderm taxa can be successfully analyzed using MRI. The achievable voxel resolution depends on the size of the specimen under study and the properties of the MRI scanner. However, pronounced artifacts must be expected in species that ingest para- or ferromagnetic sediment.

only through destructive analysis (*e.g.*, the morphology of Aristotle's lantern in sea urchins).

Equivalent to the successful studies on hard parts using µCT, MRI can be employed for the analysis of soft tissue anatomy in echinoderms. This applies to crinoids (Fig. 6A–B), asteroids (Fig. 6C–D, see also Laforsch *et al.* 2012), ophiuroids (Fig. 6E–F), as well as holothuroids (Fig. 6G–H). Large-scale scanning of sea cucumbers using MRI could be of particular interest, because µCT does not reveal many structural features in most holothuroids if applied to unstained whole specimens (Fig. 5G). However, the applicability of MRI might be limited by the currently achievable resolution and potentially pronounced artifacts caused by para- or ferromagnetic sediment located inside the specimen (Ziegler *et al.* 2011b).

The last point that I would like to stress is that due to the digital nature of the morphological data obtained using µCT and MRI, data deposition and data sharing are poised to lead to an improved transparency of anatomical findings in general. However, a prerequisite for this would be the availability of adequate voxel data repositories that permit long-term data storage and curation analogous to conventional museum specimens. These aspects are currently under debate and will hopefully be resolved in the coming years (Berquist *et al.* 2012; Rowe & Frank 2011; Ziegler *et al.* 2010a).

Conclusions

The two non-invasive tomographic imaging techniques µCT and MRI constitute powerful tools for zoomorphologists that are interested in gathering 3D datasets of whole specimens. Because of the wide-spread presence of calcified structures in echinoderms (except for most sea cucumbers), these organisms are well suited for systematic whole specimen scanning using µCT. Although exceptions do exist, for example because of artifacts related to para- or ferromagnetic inclusions, the visualization of soft part anatomy can be successfully performed in most echinoderm taxa using MRI. The broad application of non-invasive imaging techniques to echinoids has resulted in novel insight into the evolution of important organ systems such as axial complex, gastric caecum, lantern protractor muscles, and teeth—these studies would not have been undertaken using conventional destructive modalities.

Acknowledgements

I would like to thank the many curators who supplied me with hundreds of specimens that were indispensable for this large-scale imaging project. Chantal De Ridder (Brussels, Belgium), Andreas Kroh (Vienna, Austria), Rich Mooi (San Francisco, CA, USA), and Andrew B. Smith (London, UK) provided invaluable guidance with taxon selection. I am grateful to Owen Anderson (Wellington, New Zealand), Thomas Bartolomaeus (Bonn, Germany), Saskia Brauer (Bonn, Germany), Ty Hibberd (Kingston, Australia), Kathrin Fahrein (Berlin, Germany), Stephen Keable (Sydney, Australia), Kirill Minin (Moscow, Russia), Ashley Miskelly (Kurrajong, NSW, Australia), Esther Ullrich-Lüter (Berlin, Germany), Anne Zakrzewski (Bonn, Germany), and Barbara Uchańska-Ziegler & Andreas Ziegler (Berlin, Germany) for donating specimens. Felix Beckmann (Hamburg, Germany), Malte Ogurreck (Hamburg, Germany), Heiko Temming (Leipzig, Germany), Stuart R. Stock (Chicago, IL, USA), and Louis G. Zachos (Oxford, MI, USA) provided access to and help with µCT scanners. MRI scanning protocols for sea urchins were developed and applied together with Cornelius Faber

(Münster, Germany), Susanne Mueller (Berlin, Germany), and Leif Schröder (Berlin, Germany). Robert Brandt (Berlin, Germany), Thomas Heinzeller (Munich, Germany), Steffen Prohaska (Berlin, Germany), Bernhard Ruthensteiner (Munich, Germany), Thomas Steinke (Berlin, Germany), and Peter Weinert (Munich, Germany) provided helpful advice regarding 3D visualization, computation, and 3D modeling. Comments by two reviewers as well as the editors helped to improve the manuscript. This work was performed in part at the Center for Nanoscale Systems (Harvard University), which is supported by the National Science Foundation under Award No. ECS-0335765. Funding for this study was provided by the Deutsche Forschungsgemeinschaft through Grant No. ZI-1274/1–1. I am indebted to Gonzalo Giribet (Cambridge, MA, USA) for his hospitality and generous financial support.

References

Aschauer, B., Heinzeller, T. & Weinert, P. (2010) Almost within grasp: crinoid organs rendered 3-dimensionally. *In*: Harris, L.G., Böttger, S.A., Walker, C.W. & Lesser, M.P. (Eds.), *Echinoderms: Durham. Proceedings of the 12th International Echinoderm Conference, Durham, New Hampshire, USA, 7–11 August 2006.* A.A. Balkema Publishers, Leiden/London/New York/Philadelphia/Singapore, pp. 9–14.

Berquist, R.M., Gledhill, K.M., Peterson, M.W., Doan, A.H., Baxter, G.T., Yopak, K.E., Kang, N., Walker, H.J., Hastings, P.A. & Frank, L.R. (2012) The Digital Fish Library: using MRI to digitize, database, and document the morphological diversity of fish. *PLoS ONE*, 7, e34499.

Degenhardt, K., Wright, A.C, Horng, D., Padmanabhan, A. & Epstein, J.A. (2010) Rapid 3D phenotyping of cardiovascular development in mouse embryos by micro-CT with iodine staining. *Circulation: Cardiovascular Imaging*, 3, 314–322.

Dominguez, P., Jacobson, A.G. & Jefferies, R.P.S. (2002) Paired gill slits in a fossil with a calcite skeleton. *Nature*, 417, 841–844.

Faraj, K.A., Cuijpers, V.M.J.I., Wismans, R.G., Walboomers, X.F., Jansen, J.A., van Kuppevelt, T.H. & Daamen, W.F. (2009) Micro-computed tomographical imaging of soft biological materials using contrast techniques. *Tissue Engineering: Part C*, 15, 493–499.

Jakob, P. (2011) Small animal magnetic resonance imaging: basic principles, instrumentation and practical issue. *In*: Kiessling, F. & Pichler, B.J. (Eds.), *Small Animal Imaging.* Springer, Berlin, Heidelberg, pp. 151–164.

Jeffery, N.S., Stephenson, R.S., Gallagher, J.A., Jarvis, J.C. & Cox, P.G. (2011) Micro-computed tomography with iodine staining resolves the arrangement of muscle fibers. *Journal of Biomechanics*, 44, 189–192.

Kroh, A. & Mooi, R. (2011). World Echinoidea Database. Available from: http://www.marinespecies.org/echinoidea (accessed 10/2012).

Kroh, A. & Smith, A.B. (2010) The phylogeny and classification of post-Palaeozoic echinoids. *Journal of Systematic Palaeontology*, 8, 147–212.

Laforsch, C., Imhof, H., Sigl, R., Settles, M., Heß, M. & Wanninger, A. (2012) Applications of computational 3D-modeling in organismal biology. *In*: Alexandru, C. (Ed.), *Modeling and simulation in engineering*. InTech, Rijeka, pp. 117–142.

MacLeod, N., Benfield, M. & Culverhouse, P. (2010) Time to automate identification. *Nature*, 467, 154–155.

Metscher, B.D. (2009a) MicroCT for comparative morphology: simple staining methods allow high-contrast 3D imaging of diverse non-mineralized animal tissues. *BMC Physiology*, 9, 11.

Metscher, B.D. (2009b) MicroCT for developmental biology: a versatile tool for high-contrast 3D imaging at histological resolutions. *Developmental Dynamics*, 238, 632–640.

Rahman, I.A. & Clausen, S. (2009) Re-evaluating the palaeobiology and affinities of the Ctenocystoidea (Echinodermata). *Journal of Systematic Palaeontology*, 7, 413–426.

Rahman, I.A. & Zamora, S. (2009) The oldest cinctan carpoid (stem-group Echinodermata), and the evolution of the water vascular system. *Zoological Journal of the Linnean Society*, 157, 420–432.

Rolet, G., Ziegler, A. & De Ridder, C. (2012) Presence of a seawater-filled caecum in *Echinocardium cordatum* (Echinoidea: Spatangoida). *Journal of the Marine Biological Association of the United Kingdom*, 92, 379–385.

Rowe, T. & Frank, L.R. (2011) The disappearing third dimension. *Science*, 331, 712–714.

Stauber, M. & Müller, R. (2008) Micro-computed tomography: a method for the non-destructive evaluation of the three-dimensional structure of biological specimens. *Methods in Molecular Biology*, 455, 273–292.

Walter, T., Shattuck, D.W., Baldock, R., Bastin, M.E., Carpenter, A.E., Duce, S., Ellenberg, J., Fraser, A., Hamilton, N.,

Pieper, S., Ragan, M.A., Schneider, J.E., Tomancak, P. & Hériche, J.K. (2010) Visualization of image data from cells to organisms. *Nature Methods Supplement*, 7, S26–S41.

Zamora, S., Rahman, I.A. & Smith, A.B. (2012) Plated Cambrian bilaterians reveal the earliest stages of echinoderm evolution. *PLoS ONE*, 7, e38296.

Ziegler, A. & Menze, B.H. (in press) Advanced acquisition, visualization, and analysis of zoo-anatomical data. *In*: Zander, J. & Mostermann P.J. (Eds.), *Computation for Humanity*. CRC Press, Boca Raton.

Ziegler, A. & Mueller, S. (2011) Analysis of freshly fixed and museum invertebrate specimens using high-resolution, high-throughput MRI. *Methods in Molecular Biology*, 771, 633–651.

Ziegler, A., Faber, C., Mueller, S. & Bartolomaeus, T. (2008a) Systematic comparison and reconstruction of sea urchin (Echinoidea) internal anatomy: a novel approach using magnetic resonance imaging. *BMC Biology*, 6, 33.

Ziegler, A., Faber, C. & Mueller, S. (2008b) 3D visualization of sea urchin anatomy. Available from: http://www.nhm.ac.uk/research-curation/research/projects/echinoid-directory/models/ (accessed 10/2012).

Ziegler, A., Faber, C. & Bartolomaeus, T. (2009) Comparative morphology of the axial complex and interdependence of internal organ systems in sea urchins (Echinodermata: Echinoidea). *Frontiers in Zoology*, 6, 10.

Ziegler, A., Ogurreck, M., Steinke, T., Beckmann, F., Prohaska, S. & Ziegler, A. (2010a) Opportunities and challenges for digital morphology. *Biology Direct*, 5, 45.

Ziegler, A., Mooi, R., Rolet, G. & De Ridder, C. (2010b) Origin and evolutionary plasticity of the gastric caecum in sea urchins (Echinodermata: Echinoidea). *BMC Evolutionary Biology*, 10, 313.

Ziegler, A., Mietchen, D., Faber, C., von Hausen, W., Schöbel, C., Sellerer, M. & Ziegler, A. (2011a) Effectively incorporating selected multimedia content into medical publications. *BMC Medicine*, 9, 17.

Ziegler, A., Kunth, M., Mueller, S., Bock, C., Pohmann, R., Schröder, L., Faber, C. & Giribet, G. (2011b) Application of magnetic resonance imaging in zoology. *Zoomorphology*, 130, 227–254.

Ziegler A., Schröder, L., Ogurreck, M., Faber, C. & Stach, T. (2012a) Evolution of a novel muscle design in sea urchins (Echinodermata: Echinoidea). *PLoS ONE*, 7, e37520.

Ziegler, A., Stock, S.R., Menze, B.H. & Smith, A.B. (2012b) Macro- and microstructural diversity of sea urchin teeth revealed by large-scale micro-computed tomography survey. *Proceedings of SPIE*, 8506, 85061G

APPENDIX. List of sea urchin species analyzed in the course of this study. Families have been grouped according to Kroh & Smith (2010), while species names have been adapted using Kroh & Mooi (2011). Please refer to these two references for taxon authorship. Numbers in the columns 'MRI' and 'µCT' indicate the voxel resolution (in µm) of the isotropic, uncompressed dataset. '2D' refers to non-isotropic datasets with 50 x 50 x 200 µm voxel resolution. BMNH = British Museum of Natural History, London, UK; CASIZ = California Academy of Sciences Invertebrate Zoology, San Francisco, CA, USA; MCZ = Museum of Comparative Zoology, Cambridge, MA, USA; MNHN = Muséum national d'Histoire naturelle, Paris, France; NHMW = Naturhistorisches Museum Wien, Vienna, Austria; NIWA = National Institute of Water & Atmospheric Research, Wellington, New Zealand; USNM = National Museum of Natural History, Washington, DC, USA; ZMB = Systematische Zoologie am Museum für Naturkunde, Berlin, Germany; ZMH = Zoologisches Institut und Museum Hamburg, Germany; ZMK = Zoologisk Museum København, Copenhagen, Denmark; ZSM = Zoologische Staatssammlung München, Munich, Germany.

Family	Species	MRI	Specimen No.	µCT	Specimen No.
Histocidaridae	*Histocidaris elegans*	81	ZMH E307	16	ZMH E307
	Histocidaris purpurata	-	-	16.07	ZMH E309
Ctenocidaridae	*Aporocidaris incerta*	-	-	13.91	ZMH E8038
	Aporocidaris milleri	-	-	13.91	ZMB Ech 5412
	Ctenocidaris nutrix	79	BMNH 1956.10.5.1	14	BMNH 1956.10.5.1
	Ctenocidaris perrieri	-	-	12.61	MCZ 8379
	Notocidaris gaussensis	79	ZMB Ech 5456	14	ZMB Ech 5456
	Rhynchocidaris triplopora	-	-	13.91	ZMB Ech 5460
Cidaridae	*Acanthocidaris hastingeria*	-	-	13.91	ZMB Ech 5874
	Austrocidaris canaliculata	79	ZMB Ech 2244	13.39	ZMB Ech 2244
	Calocidaris micans	-	-	35.01	MCZ 283
	Centrocidaris doederleini	-	-	9.78	MCZ187
	Cidaris cidaris	81	BMNH 1925.10.30.103-113	18.87	BMNH 1925.10.30.103-113

Family	Species	MRI	Specimen No.	µCT	Specimen No.
	Cidaris nuda	-	-	20	ZMB Ech 2167
	Compsocidaris pyrsacantha	-	-	29.64	MCZ 7861
	Eucidaris metularia	44	BMNH 1969.5.1.15-40	13.91	BMNH 1969.5.1.15-40
	Eucidaris thouarsii	2D	ZMB Ech 1369	13.91	ZMB Ech 1369
	Eucidaris tribuloides	2D	ZMB Ech 5474	13.91	ZMB Ech 5474
	Goniocidaris biserialis	-	-	13.91	ZMB Ech 6764
	Goniocidaris tubaria	-	-	9.82	ZMH E288
	Hesperocidaris panamensis	2D	ZMB Ech 5407	13.91	ZMB Ech 5407
	Ogmocidaris benhami	-	-	12.78	MCZ 984
	Phyllacanthus imperialis	-	-	13.39	ZMB Ech 6513
	Plococidaris verticillata	-	-	15	ZMH E305
	Prionocidaris bispinosa	-	-	18.57	ZMH E267
	Rhopalocidaris gracilis	-	-	12.08	MCZ 4860
	Stereocidaris indica	79	ZMB Ech 7364	16.07	ZMB Ech 7364
	Stylocidaris affinis	-	-	14.62	MCZ 234
	Tretocidaris bartletti	-	-	11.3	MCZ 4561
Psychocidaridae	*Psychocidaris ohshimai*	79	NHMW 2010/0240/0001	15	NHMW 2010/0240/0001
Kamptosomatidae	*Kamptosoma asterias*	-	-	7	CASIZ 182429
Phormosomatidae	*Phormosoma bursarium*	-	-	15.7	MCZ 911
	Phormosoma placenta	-	-	13.91	USNM E17633
Echinothuriidae	*Araeosoma belli*	-	-	15.15	MCZ 7765
	Asthenosoma varium	-	-	19.64	ZMH E3
	Calveriosoma gracile	-	-	15	BMNH 1881.11.22.21
	Hapalosoma pellucidum	-	-	22.42	MCZ 6094
	Hygrosoma petersii	-	-	25.61	MCZ 2970
	Sperosoma obscurum	-	-	20	MCZ 903
	Tromikosoma uranus	-	-	23.57	BMNH 1976.7.30.74
Micropygidae	*Micropyga tuberculata*	81	BMNH 98.8.8.45/6	13.91	BMNH 98.8.8.45/6
Diadematidae	*Astropyga radiata*	-	-	8.21	ZMB Ech 3877
	Centrostephanus coronatus	-	-	9.82	CASIZ 100820
	Centrostephanus longispinus	66	BMNH 1952.3.26.64-8	13.91	BMNH 1952.3.26.64-8
	Chaetodiadema granulatum	-	-	20.53	NHMW 10745
	Chaetodiadema pallidum	-	-	20	CASIZ 98074
	Diadema antillarum	2D	ZMB Ech 4374	13.91	CASIZ 98084
	Diadema ascensionis	-	-	13.39	BMNH 1972.8.22.50-52
	Diadema savignyi	40	ZMB Ech 7411	13.91	ZMB Ech 7411
	Diadema setosum	2D	ZMB Ech 4814	13.91	NHMW 10755
	Echinothrix diadema	2D	ZMB Ech 2346	13.39	ZMB Ech 2346
	Eremopyga denudata	-	-	43.56	MCZ 685

Family	Species	MRI	Specimen No.	µCT	Specimen No.
	Lissodiadema lorioli	-	-	8.2	CASIZ 103520
Aspidodiadematidae	*Aspidodiadema arcitum*	-	-	9.82	USNM 27568
	Aspidodiadema hawaiiense	81	USNM 27590	13.91	USNM 27588
	Aspidodiadema tonsum	-	-	9.82	BMNH 81.11.22.24
	Plesiodiadema horridum	-	-	8	MCZ 607
	Plesiodiadema indicum	81	ZMB Ech 7232	13.91	ZMB Ech 7232
Pedinidae	*Caenopedina mirabilis*	81	USNM 31182	13.91	USNM 31182
	Caenopedina otagoensis	-	-	8.2	ZMB Ech 7403
	Caenopedina porphyrogigas	-	-	20.53	ZMB Ech 7404
Saleniidae	*Salenia goesiana*	81	USNM 10649	8.87	USNM 14581
	Salenocidaris hastigera	81	ZMB Ech 5816	13.91	ZMB Ech 5816
	Salenocidaris varispina	-	-	7.4	MCZ 4883
Stomopneustidae	*Stomopneustes variolaris*	81	USNM E45930	13.91	USNM E45930
Glyptocidaridae	*Glyptocidaris crenularis*	90	ZSM 20011444	23.38	ZSM 20011444
Arbaciidae	*Arbacia dufresnii*	2D	ZMB Ech 2222	13.91	ZMB Ech 2222
	Arbacia lixula	44	BMNH 1952.3.26.31-36	13.91	BMNH 1966.5.6.57-65
	Arbaciella elegans	-	-	6.11	ZMH E185
	Coelopleurus sp.	-	-	13.91	ZMB Ech 7412
	Dialithocidaris gemmifera	-	-	10.92	MCZ 8317
	Habrocidaris scuttata	-	-	6.3	MCZ 7787
	Podocidaris sp.	-	-	9.82	ZMB Ech 7409
	Pygmaeocidaris prionigera	-	-	6.05	MCZ 8741
	Tetrapygus niger	2D	ZMB Ech 1346	19.27	ZMH E198
Parasaleniidae	*Parasalenia gratiosa*	79	BMNH 1983.2.15.7	14	BMNH 1983.2.15.7
Temnopleuridae	*Amblypneustes pallidus*	2D	ZMB Ech 6334	13.91	ZMB Ech 6334
	Erbechinus spectabilis	-	-	18.56	MCZ 4955
	Holopneustes inflatus	2D	ZMB Ech 2639	13.91	ZMB Ech 2639
	Mespilia globulus	44	ZMB Ech 5620	13.91	ZMB Ech 5620
	Microcyphus rousseaui	-	-	19.64	ZMH E4143
	Opechinus variabilis	-	-	6.69	MCZ 3944
	Pseudechinus magellanicus	2D	ZMB Ech 2188	13.91	BMNH 1967.4.3.24-25
	Salmaciella oligopora	-	-	35.82	MCZ 4283
	Salmacis sphaeroides	2D	ZMB Ech 4337	16.43	NHMW 10786
	Temnopleurus hardwickii	-	-	20	NHMW 10772
	Temnopleurus michaelseni	2D	ZMB Ech 6331	-	-
	Temnopleurus reevesii	2D	ZMB Ech 3588	13.91	BMNH 1981.2.6.55-56
	Temnopleurus toreumaticus	2D	ZMB Ech 2802	13.91	ZMB Ech 2802
	Temnotrema elegans	-	-	8.2	ZMB Ech 6332
Trigonocidaridae	*Desmechinus rufus*	-	-	12.25	MCZ 4735
	Genocidaris maculata	36	ZMB Ech 5827	9.82	ZSM 20011685
	Hypsiechinus coronatus	-	-	3.86	MCZ 1400

Family	Species	MRI	Specimen No.	µCT	Specimen No.
	Prionechinus sagittiger	-	-	5.5	ZMB Ech 6498
	Trigonocidaris albida	32	ZSM 20012468	10	ZSM 20012468
Echinidae	*Dermechinus horridus*	-	-	24.37	MCZ 4252
	Echinus esculentus	81	ZMB Ech 3826	13.91	ZMB Ech 3826
	Gracilechinus acutus	2D	ZMB Ech 3714	13.91	NHMW 10833
	Gracilechinus affinis	-	-	15.71	ZMH E7707
	Gracilechinus alexandri	2D	ZMB Ech 4340	13.91	ZMB Ech 4340
	Polyechinus agulhensis	2D	ZMB Ech 7219	13.91	ZMB Ech 7219
	Sterechinus agassizii	79	BMNH 1914.8.12.126-127	13.91	BMNH 1914.8.12.126-7
	Sterechinus antarcticus	2D	ZMB Ech 5439	-	-
	Sterechinus neumayeri	2D	ZMB Ech 5442	13.91	ZMB Ech 5442
Parechinidae	*Loxechinus albus*	2D	BMNH 1966.5.1.61-75	16	BMNH 1966.9.27.35
	Paracentrotus lividus	81	ZMB Ech 7406	13.39	ZMB Ech 7406
	Parechinus angulosus	2D	ZMB Ech 5644	13.91	NHMW 10869
	Psammechinus microtuberculatus	2D	ZMB Ech 4770	13.91	ZMB Ech 4770
	Psammechinus miliaris	44	Author's collection	13.91	ZMB Ech 2011
Toxopneustidae	*Gymnechinus robillardi*	79	BMNH 1890.6.27.5-8	13.91	BMNH 1890.6.27.5-8
	Lytechinus variegatus	81	ZMB Ech 5517	13.91	ZMB Ech 7408
	Nudechinus scotiopremnus	2D	ZMB Ech 6130	13.91	ZMB Ech 6130
	Nudechinus verruculatus	-	-	9.82	ZMH E506
	Pseudoboletia indiana	-	-	21.43	NHMW 10830
	Sphaerechinus granularis	81	ZMB Ech 2366	13.91	ZMB Ech 2366
	Toxopneuses pileolus	2D	ZMB Ech 3871	9.82	ZMB Ech 3871
	Tripneustes gratilla	-	-	19.64	ZMB Ech 1527
	Tripneustes ventricosus	2D	ZMB Ech 5498	13.91	ZMB Ech 5498
Strongylocentrotidae	*Hemicentrotus pulcherrimus*	2D	ZMB Ech 6425	13.91	NHMW 10893
	Mesocentrotus franciscanus	-	-	22	MCZ 7313
	Pseudocentrotus depressus	2D	ZMB Ech 6426	13.91	ZMB Ech 6426
	Strongylocentrotus droebachiensis	2D	ZMB Ech 4422	12.5	BMNH 1969.6.12.512-522
	Strongylocentrotus fragilis	-	-	30.39	MCZ 4086
	Strongylocentrotus purpuratus	42	CASIZ 5724	13.91	CASIZ 5724
Echinometridae	*Caenocentrotus gibbosus*	2D	ZMB Ech 5405	13.91	ZMB Ech 5405
	Colobocentrotus atratus	2D	ZMB Ech 4985	25	NHMW 10960
	Colobocentrotus mertensii	-	-	35.89	MCZ 2136
	Echinometra lucunter	-	-	19.27	NHMW 10928
	Echinometra mathaei	81	BMNH 1969.5.1.61-75	13.91	BMNH 1969.5.1.61-75
	Echinometra mathaei oblonga	2D	ZMB Ech 3862	13.91	ZMB Ech 3862
	Echinometra viridis	2D	ZMB Ech 5503	-	-
	Echinostrephus molaris	2D	ZMB Ech 4000	13.91	ZMB Ech 4000
	Evechinus chloroticus	-	-	30	NHMW 10898

Family	Species	MRI	Specimen No.	µCT	Specimen No.
	Heliocidaris australiae	-	-	13.91	ZMH E7966
	Heliocidaris crassispina	2D	ZMB Ech 6424	13.91	ZMB Ech 6424
	Heliocidaris erythrogramma	2D	ZMB Ech 5745	13.91	ZMB Ech 5745
	Heterocentrotus mammillatus	2D	ZMB Ech 1567	13.91	ZMB Ech 1567
	Zenocentrotus paradoxus	-	-	20.34	MCZ 6004
Echinoneidae	*Echinoneus cyclostomus*	66	BMNH 1969.5.1.105	13.91	BMNH 1969.5.1.105
Apatopygidae	*Apatopygus recens*	-	-	8.62	ZMK Mortensen coll'n
Cassidulidae	*Cassidulus caribaearum*	81	CASIZ 112632	8.87	ZMK Mortensen coll'n
	Rhyncholampas pacificus	-	-	22	ZMH E755
Neolampadidae	*Neolampas rostellata*	-	-	9	MNHN EcEh330
Echinolampadidae	*Echinolampas depressa*	81	USNM E32955	13.91	USNM E32955
Clypeasteridae	*Ammotrophus cyclius*	-	-	20.61	MCZ 7005
	Arachnoides placenta	81	ZMB Ech 1439	13.91	ZMB Ech 1439
	Clypeaster fervens	-	-	18.57	BMNH 1948.12.9.15-16
	Clypeaster reticulatus	81	USNM 34282	13.91	USNM 34282
	Clypeaster rosaceus	96	ZMB Ech 2520	17	ZMB Ech 2520
	Fellaster zelandiae	-	-	23.57	ZMB Ech 7402
Echinocyamidae	*Echinocyamus pusillus*	20	ZMB Ech 7410	9	ZMB Ech 7410
	Mortonia australis	-	-	8	CASIZ 108132
Fibulariidae	*Fibularia ovulum*	36	USNM E35308	6.82	USNM E35308
	Fibulariella acuta	-	-	3.8	CASIZ 188798
Laganidae	*Jacksonaster depressum*	86	BMNH 1932.4.28.227-34	13.91	BMNH 1932.4.28.227-34
	Laganum decagonale	-	-	19.28	BMNH 79.1.2.3
	Laganum joubini	44	BMNH 1979.1.25.52-60	13.91	BMNH 1979.1.25.52-60
	Laganum laganum	81	USNM E09175	13.91	USNM E09175
	Peronella japonica	-	-	25.71	CASIZ 94528
	Peronella lesueuri	81	MNHN EcEh79	13.91	MNHN EcEh79
	Peronella orbicularis	81	MNHN EcEh77	13.91	MNHN EcEh77
Rotulidae	*Heliophora orbicularis*	-	-	25	ZMH E6864
	Rotula deciesdigitatus	81	ZMB Ech 2169	27.03	ZMH E742
Taiwanasteridae	*Marginoproctus sp.*	-	-	4.12	USNM Acc. 357890
Echinarachniidae	*Echinarachnius parma*	44	BMNH 55.10.3.125	13.91	ZSM 20011676
	Sinaechinocyamus mai	-	-	4.6	CASIZ 188797
Dendrasteridae	*Dendraster excentricus*	-	-	22.86	ZMB Ech 7400
Scutellidae	*Scaphechinus mirabilis*	-	-	13.91	ZMB Ech 7405
Astriclypeidae	*Astriclypeus manni*	-	-	36.48	MCZ 7300
	Echinodiscus auritus	-	-	22.86	ZMB Ech 2647
	Echinodiscus bisperforatus	-	-	19.44	BMNH 1964.10.13.20-23
Mellitidae	*Encope micropora*	-	-	20.38	MCZ 2625
	Leodia sexiesperforata	-	-	18.78	MCZ 4460

Family	Species	MRI	Specimen No.	µCT	Specimen No.
	Mellita isometra	-	-	29.37	ZMH E737
	Mellita quinquiesperforata	-	-	25.71	ZMB Ech 7401
	Mellitella stokesii	-	-	13.91	USNM E40733
Calymnidae	-	-	-	-	-
Corystusidae	-	-	-	-	-
Urechinidae	*Antrechinus mortenseni*	81	ZMH E7381	13.91	ZMH E7381
	Urechinus naresianus	81	ZSM 20012380	13.91	ZMK Mortensen coll'n
Plexechinidae	*Plexechinus planus*	-	-	13.91	ZMH E7345
Pourtalesiidae	*Pourtalesia jeffreysi*	81	ZSM 20011456	13.91	ZSM 20011456
	Pourtalesia wandeli	86	BMNH 1976.7.30.76-95	16.6	BMNH 1976.7.30.76-95
Palaeostomatidae	-	-	-	-	-
Hemiasteridae	-	-	-	-	-
Micrasteridae	-	-	-	-	-
Aeropsidae	*Aeropsis rostrata*	-	-	9.3	ZMK Mortensen coll'n
Schizasteridae	*Abatus cavernosus*	81	ZMB Ech 5854	-	-
	Abatus cordatus	-	-	13.91	ZSM 20011462
	Brisaster fragilis	-	-	13.91	ZMK Mortensen coll'n
	Moira atropos	-	-	17.39	ZMB Ech 5491
	Schizaster lacunosus	-	-	16.67	ZMB Ech 3551
Prenasteridae	-	-	-	-	-
Pericosmidae	-	-	-	-	-
Paleopneustidae	*Plesiozonus hirsutus*	-	-	64.45	CASIZ 186314
Palaeotropidae	*Palaeobrissus hilgardi*	-	-	23.38	CASIZ 112853
Brissidae	*Brissopsis luzonica*	-	-	15	ZSM 20011858
	Brissopsis lyrifera	-	-	20	ZMB Ech 4841
	Brissus unicolor	-	-	23.57	ZMB Ech 1371
	Metalia sp.	-	-	19.28	ZMB Ech 5019
Spatangidae	*Spatangus purpureus*	81	ZMB Ech 3236	13.91	ZMB Ech 3236
Eupatagidae	-	-	-	-	-
Eurypatagidae	-	-	-	-	-
Maretiidae	*Maretia planulata*	-	-	13.91	ZMB Ech 2127
	Nacospatangus alta	81	ZSM 20011608	13.91	ZSM 20011608
Macropneustidae	-	-	-	-	-
Loveniidae	*Echinocardium cordatum*	81	ZMB Ech 7407	13.91	ZMB Ech 7407
	Echinocardium flavescens	-	-	13.91	ZSM 20011403/1
	Echinocardium pennatifidum	-	-	13.91	ZSM 20011401
	Lovenia subcarinata	-	-	15	ZSM 20011447
Incerta sedis	*Amphipneustes lorioli*	-	-	24	ZMH E7354
	Brachysternaster chesheri	-	-	22	ZMH E7356
	Parapneustes cordatus	-	-	13.91	ZMH E7358